Monthly Notices of Royal Astronomical Society 476.1 (2015): 476-483

DOI: 10.1093/mnras/stv2335

Mon. Not. R. Astron. Soc. **000**, 1–8 (2010) Printed 14 October 2015 (MN LATEX style file v2.2)

The distribution of mass components in simulated disc galaxies

Isabel M. Santos-Santos[1,2⋆], Chris B. Brook[1,2], Greg Stinson[3], Arianna Di Cintio[4], James Wadsley[5], Rosa Domínguez-Tenreiro[1,2], Stefan Gottlöber[6], Gustavo Yepes[1,2]
[1]*Departamento de Física Teórica, Universidad Autónoma de Madrid, 28049 Cantoblanco, Madrid, Spain*
[2]*Astro-UAM, UAM, Unidad Asociada CSIC*
[3]*Max-Planck-Institut für Astronomie, Königstuhl 17, Heidelberg, 69117, Germany*
[4]*Dark Fellow, Dark Cosmology Centre, NBI, University of Copenhagen, Juliane Maries Vej 30, DK-2100 Copenhagen, Denmark*
[5]*Department of Physics & Astronomy, McMaster University, Hamilton, Ontario, L8S 4M1, Canada*
[6]*Leibniz Institute for Astrophysics Potsdam, An der Sternwarte 16, 14482 Potsdam, Germany*

Accepted XXXX . Received XXXX; in original form XXXX

ABSTRACT

Using 22 hydrodynamical simulated galaxies in a ΛCDM cosmological context we recover not only the observed baryonic Tully-Fisher relation, but also the observed "mass discrepancy–acceleration" relation, which reflects the distribution of the main components of the galaxies throughout their disks. This implies that the simulations, which span the range $52<V_{\rm flat}<222\,{\rm km\,s^{-1}}$ where $V_{\rm flat}$ is the circular velocity at the flat part of the rotation curve, and match galaxy scaling relations, are able to recover the observed relations between the distributions of stars, gas and dark matter over the radial range for which we have observational rotation curve data. Furthermore, we explicitly match the observed baryonic to halo mass relation for the first time with simulated galaxies. We discuss our results in the context of the baryon cycle that is inherent in these simulations, and with regards to the effect of baryonic processes on the distribution of dark matter.

Key words: galaxies: evolution - formation - haloes cosmology: theory - dark matter

1 INTRODUCTION

Within a ΛCDM context, the angular momentum of disc galaxies originates from tidal torques imparted by surrounding structures in the expanding Universe, prior to proto-galactic collapse (Peebles 1969; Barnes & Efstathiou 1987). Assuming that gas gains a similar amount of angular momentum as the dark matter, and that angular momentum is substantially retained as the gas cools to the centres of dark matter halos (Fall & Efstathiou 1980), then the gas will settle into a disc, fragment and form stars.

Simulations have shown that angular momentum acquisition is more complicated than this picture, involving a complex web structure (e.g. Pichon et al. 2011; Domínguez-Tenreiro et al. 2015). Indeed, there has been significant progress over the past years in our ability to simulate the processes of disc formation within a cosmological context. Without an efficient feedback scheme, angular momentum is lost to dynamical friction during the mergers of overly dense sub-structures (e.g. Navarro & Steinmetz 2000; Maller & Dekel 2002; Piontek & Steinmetz 2011).

Progress was made by implementing increasingly effective recipes for feedback from supernovae (Thacker & Couchman 2001; Stinson et al. 2006) and the inclusion of other forms of feedback from massive stars (Stinson et al. 2013; Hopkins et al. 2014). The benchmark for assessing this progress has primarily been the ability to match the Tully-Fisher relation (e.g. Governato et al. 2004; Doménech-Moral et al. 2012), with recent simulations succeeding at this, and in particular matching the Baryonic Tully Fisher relation (BTFR), for galaxies over a range of masses (Brook et al. 2012b; Aumer et al. 2013).

Yet rotation curves of observed galaxies provide significantly more information regarding the angular momentum of galaxies than is contained within the BTFR, allowing more stringent constraints on galaxy formation models which have not previously been applied to simulated galaxies. High resolution observations of HI velocities, combined with studies of the gas and stellar mass distributions, provide detailed information on how the different mass components are radially distributed in galaxies with a wide range of rotational velocities V_r (e.g. Begeman et al. 1991; Sanders & Verheijen 1998; de Blok et al. 2001; Gentile et al. 2004; Kuzio de Naray et al. 2006; Oh et al. 2015).

Differences between the mass implied by measured rotational

⋆ E-mail: isabelm.santos@uam.es

Table 1. Properties of the simulated galaxies ordered by halo mass. MaGICC galaxies have a "g" as prefix, while CLUES galaxies have a "C". Disk scale lengths h and central surface brightnesses μ_0 are derived from exponential fits to the surface brightness profile in the I band.

Name	$M_{\rm halo}$ ($M_\odot$)	M_* ($M_\odot$)	$M_{\rm HI}$ ($M_\odot$)	h (kpc)	μ_0 (mag as^{-1})	$V_{\rm max}$ (km s^{-1})	$V_{\rm flat}$ (km s^{-1})
g15784_MW	1.49×10^{12}	5.67×10^{10}	1.96×10^{10}	3.23	19.09	222.10	222.10
g21647_MW	8.24×10^{11}	2.51×10^{10}	5.62×10^{9}	1.30	17.39	189.79	163.84
g1536_MW	7.06×10^{11}	2.36×10^{10}	6.78×10^{9}	3.46	20.54	175.95	175.95
g5664_MW	5.39×10^{11}	2.74×10^{10}	4.19×10^{9}	2.34	19.51	196.66	151.40
g7124_MW	4.47×10^{11}	6.30×10^{9}	3.49×10^{9}	2.79	20.60	120.14	120.14
g15807_Irr	2.82×10^{11}	1.46×10^{10}	4.68×10^{9}	1.94	18.68	141.21	141.21
g15784_Irr	1.70×10^{11}	4.26×10^{9}	2.70×10^{9}	2.27	20.30	106.90	106.90
g22437_Irr	1.10×10^{11}	7.44×10^{8}	1.08×10^{9}	1.88	21.33	75.40	75.40
g21647_Irr	9.65×10^{10}	1.98×10^{8}	3.68×10^{8}	1.75	22.77	60.85	60.85
g1536_Irr	8.04×10^{10}	4.46×10^{8}	4.39×10^{8}	1.70	21.75	67.16	67.16
g5664_Irr	5.87×10^{10}	2.36×10^{8}	2.56×10^{8}	1.66	22.28	59.50	59.50
g7124_Irr	5.23×10^{10}	1.32×10^{8}	2.30×10^{8}	1.16	21.61	52.77	52.77
C1	7.23×10^{11}	1.45×10^{10}	3.86×10^{9}	1.56	19.56	168.83	127.10
C2	5.31×10^{11}	1.11×10^{10}	6.32×10^{8}	1.83	20.40	123.59	123.59
C3	2.67×10^{11}	5.08×10^{9}	2.79×10^{9}	2.25	21.22	119.75	119.75
C4	1.87×10^{11}	4.18×10^{9}	9.77×10^{7}	1.45	20.07	101.21	101.21
C5	1.51×10^{11}	4.54×10^{9}	2.42×10^{9}	1.35	20.30	116.63	116.63
C6	1.29×10^{11}	2.08×10^{9}	2.74×10^{9}	1.53	21.29	101.66	101.66
C7	1.18×10^{11}	1.57×10^{9}	9.10×10^{8}	1.48	20.44	88.89	72.92
C8	1.21×10^{11}	1.57×10^{9}	6.34×10^{8}	1.03	20.19	85.22	85.22
C9	8.04×10^{10}	1.10×10^{9}	1.05×10^{8}	1.55	22.64	70.85	70.85
C10	6.44×10^{10}	3.78×10^{8}	6.33×10^{7}	0.86	21.55	53.35	53.35

velocities, and the baryonic mass observed in the form of gas and stars, is usually attributed to dark matter (Rubin & Ford 1970), an assumption which our simulations embrace. In this study we aim to determine whether galaxies simulated in a ΛCDM universe can reproduce the detailed radial mass distribution of observed galaxies.

An instructive way to display the radial mass distribution of a population of disc galaxies is to plot the mass discrepancy-acceleration relation (Sanders & McGaugh 2002; McGaugh 2004). Mass discrepancy, D, is defined as the ratio of the square of the measured rotation velocity, and the square of the rotation velocity that can be attributed to baryons, $D\equiv(V_r/V_b)^2$. The acceleration is defined at each radius, r, by the baryonic contribution to the centripetal acceleration, $g_b\equiv {V_b}^2/r$.

Despite a large variety in rotation curve shapes (e.g. Zwaan et al. 1995; Tully & Verheijen 1997; Swaters et al. 2009), disc galaxies with a wide range of V_r show a remarkably tight D-g_b relation (McGaugh 2004, 2014). Galaxies that present the same mass discrepancy at various radii all experience, at those radii, the same gravitational radial force as contributed by their baryons; it is as though the rotation velocity attributed to dark matter depends only on the distribution of baryonic mass. Indeed, this tight relation has been interpreted as being causal (Sanders & McGaugh 2002; McGaugh 2014), and therefore evidence for modified Newtonian dynamics, MOND (Milgrom 1983). This empirical result has no *a priori* explanation in a ΛCDM cosmology, but a study of semi-analytic models (van den Bosch & Dalcanton 2000) found that galaxies tuned to match the Tully-Fisher relation reveal a characteristic acceleration.

Here, we explore the D-g_b relation in a suite of 22 disk galaxies simulated within a ΛCDM context, which vary in their virial, stellar and baryonic masses ($M_{\rm halo}$, M_*, $M_{\rm b}$), star formation histories, disk scale lengths, central surface brightnesses and circular velocity curve shapes. As we show, the suite of galaxies tightly match the empirical M_*-$M_{\rm halo}$ (Guo et al. 2010; Moster et al. 2010), $M_{\rm b}$-$M_{\rm halo}$ (Papastergis et al. 2012) and BTFRs (McGaugh 2005).

It is important to emphasise that these simulated galaxies were not tuned to reproduce the BTFR, with free parameters tuned to match the stellar to halo mass relation at one halo mass (Brook et al. 2012b; Stinson et al. 2013), and then fixed in simulations of different mass halos. The simulations have previously been shown to match a wide range of scaling relations including the Tully-Fisher, luminosity-size, mass-metallicity relations, and HI mass to r band luminosity ratio as a function of R band magnitude, at z=0 (Brook et al. 2012b). Further, the simulations match the evolution of the stellar mass-halo mass relation (Stinson et al. 2013; Kannan et al. 2013), as derived by abundance matching (Moster et al. 2013) and a range of relations at high redshift (Obreja et al. 2014). The simulations also expel sufficient metals to match local observations (Prochaska et al. 2011; Tumlinson et al. 2011) of OVI in the circum-galactic medium (Stinson et al. 2012; Brook et al. 2012b).

The paper is organized as follows. Section 2 presents the simulations used, describing their initial conditions and baryonic modelling. The circular velocity curves, BTFR, M_*-$M_{\rm halo}$ $M_{\rm b}$-$M_{\rm halo}$ relations and plots of D versus g and radius are shown in Section 3. Residuals around the D-g relation are also shown. Finally, Section 4 discusses the implications of our results.

2 THE SIMULATIONS

Two sets of simulated galaxies have been used, with slightly different input physics, as we will explain. In first place, we use 12 galaxies from the MaGICC (Making Galaxies in a Cosmological Context) project (Brook et al. 2012a; Stinson et al. 2013). These are zoomed-in regions of a total cosmological volume of side 68 Mpc. The resolution varies depending on the "type" of simulated galaxy, labelled MilkyWay or Irregular. The former have

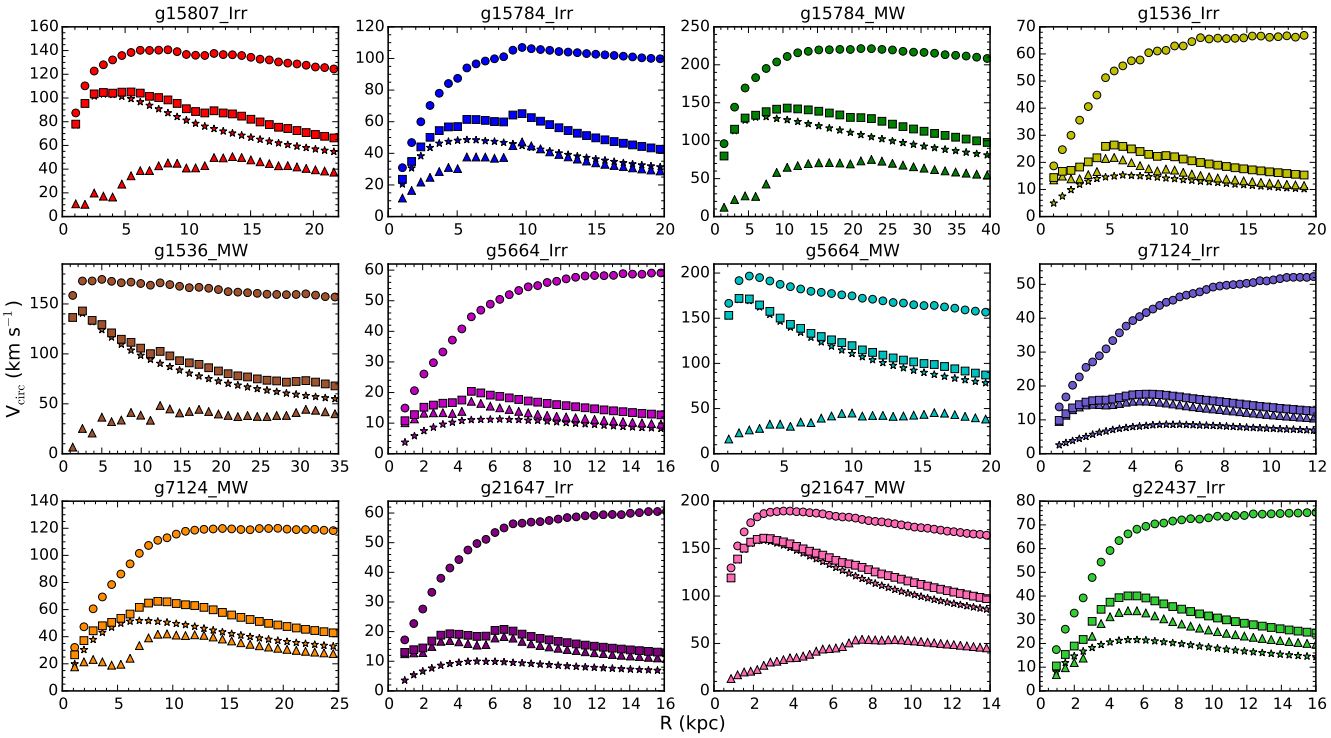

Figure 1. The circular velocity curves of the 12 MaGICC disk galaxies. Different symbols represent the velocity values due to different mass components (triangles: cold gas; stars: stars; squares: all baryons; circles: total). Simulations reproduce the variety of observed rotation curves. Furthermore, like in observations, the features present in the baryonic curves are reflected in the total one.

m_{star}=4.0×10^{4}M$_\odot$, m_{gas}=5.7×10^{4}M$_\odot$, m_{dm}=1.1×10^{6}M$_\odot$ and a gravitational softening length of ϵ=312pc (for all particle types), while the latter are more highly resolved with m_{star}=4.3×10^{3}M$_\odot$, m_{gas}=7.1×10^{3}M$_\odot$, m_{dm}=1.4×10^{5}M$_\odot$ and ϵ=156pc. The initial power spectrum of density fluctuations is derived from the McMaster Unbiased Galaxy Simulations (MUGS) (Stinson et al. 2010) which use a ΛCDM cosmology with WMAP3 parameters, i.e. $H_0 = 73$ km s^{-1} Mpc^{-1}, $\Omega_m = 0.24$, $\Omega_\Lambda = 0.76$, $\Omega_{baryon} = 0.04$ and $\sigma_8 = 0.76$.

The second set of galaxies is from a single simulation with initial conditions from the CLUES project (Constrained Local UniversE Simulations, Gottloeber et al. 2010; Yepes et al. 2014). Again the zoom-in technique is used, this time together with observational data (masses of nearby X-ray clusters and peculiar velocities obtained from catalogs) imposed as constraints on the initial conditions, in order to simulate a cosmological volume that is representative of our local universe. The Hoffman-Ribak algorithm, using the observational data mentioned above, is used to constrain scales down to $\approx 5h^{-1}$Mpc. This way structures like the Virgo cluster, Coma cluster and Great attractor, are always reproduced by the simulations.

On smaller scales, the distribution of structure is essentially random, and several dark matter-only realizations are run until a Local Group analogue (a Milky Way-M31 like binary group) is found. Then this Local Group region is re-simulated with baryons and at a higher resolution. In this case, the re-simulation includes 4096^3 effective particles in a spherical volume of $2h^{-1}$Mpc around the Local Group. The mass resolution of particles is m_{star}=1.3×10^{4}M$_\odot$, m_{gas}=1.8×10^{4}M$_\odot$ and m_{dm}=2.9×10^{5}M$_\odot$, and the gravitational softening lengths are ϵ_{bar}=223pc between baryons and ϵ_{dm}=486pc between dark matter particles. This CLUES simulation also follows a WMAP3 cosmological model.

The CLUES simulation used is not one of the previously published CLUES simulations, which were evolved using the PMTree-SPH MPI code GADGET2, but rather part of a new set with the same initial conditions but different physics prescriptions for star formation and feedback, as explained below.

All simulations in this study are evolved using the parallel N-body+SPH tree-code GASOLINE (Wadsley et al. 2004), which includes gas hydrodynamics and cooling, star formation, energy feedback and metal enrichment to model structure formation. We describe here the most important implementations (for details see Governato et al. 2010 and Stinson et al. 2013).

When gas gets cold and dense, stars are formed according to a Schmidt law with star formation rate $\propto \rho^{1.5}$. Stars feed energy and metals to the surrounding interstellar medium. Energy feedback by supernovae is implemented by means of the blastwave formalism (Stinson et al. 2006) where $\epsilon_{SN} \times 10^{51}$ erg of thermal energy is released. The amount of metals deposited from SNe explosions is computed from a Chabrier IMF, and they diffuse between gas particles as described in Shen et al. (2010). GASOLINE also accounts for the effect of a uniform background radiation field on the ionization and excitation state of the gas. In the case of the MaGICC simulations, metal-line cooling (Shen et al. 2010) and early stellar feedback from massive stars (Stinson et al. 2013) prior to their explosion as SNe are also included.

The CLUES simulations follow the physics used in Governato et al. (2010) and Guedes et al. (2011), which formed realistic dwarf and Milky Way galaxies respectively. These runs do not include metal line cooling, nor do they include early stellar feedback. As argued in Feldmann & Mayer (2015), gas cooling is also affected

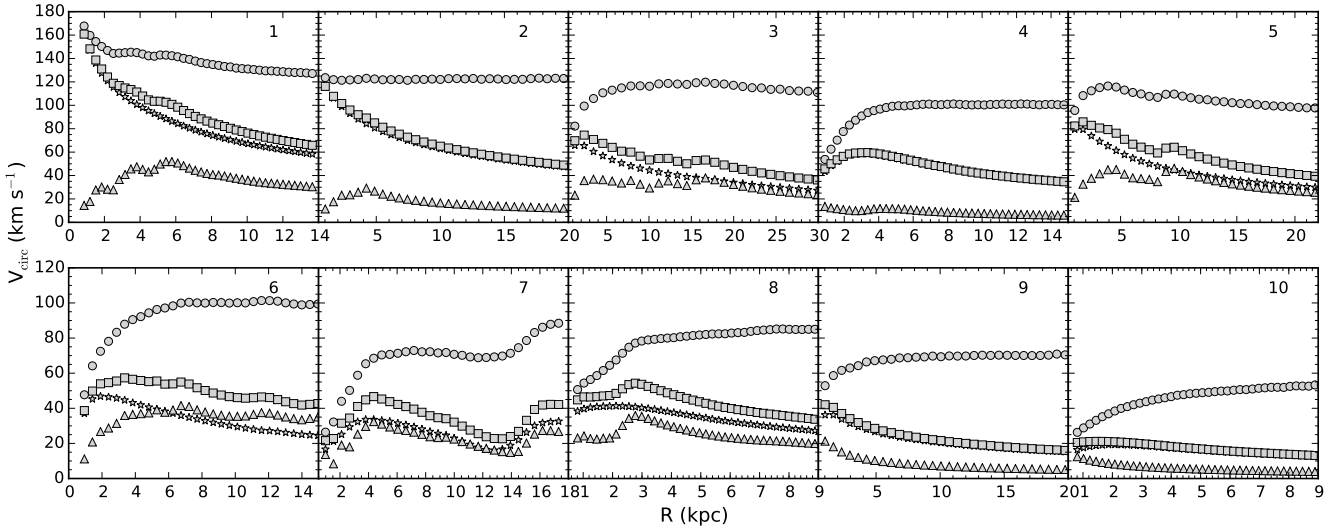

Figure 2. The circular velocity curves of the 10 galaxies selected from the CLUES simulation. Triangles: cold gas; stars: stars; squares: all baryons; circles: total.

by UV and soft X-ray emission from nearby massive stars (e.g. Cantalupo 2010; Kannan et al. 2014); it is not clear whether adding metal line cooling, without their potential counterparts, such as radiative ionization by local sources, results in a better model.

Further, in these types of simulations, feedback recipes are not well constrained, but are basically tuned to balance whatever cooling rate is included, in order to match the constraints imposed; in these simulations, constraints come from the stellar to halo mass relation. The lower cooling rates of the CLUES set of simulations is compensated by the lack of early stellar feedback, resulting in our two sets of simulations following very similar trends in their structural properties, as we will see below. One could argue that sub grid local feedback processes are included in the CLUES simulation by adjusting the cooling function.

We emphasise that the two sets of simulations share the same implementations of SNe feedback and star formation. Yet there are differences in cooling and feedback, which will result in differences in the amount of gas cycling through central regions of the galaxies. We will comment on some systematic differences between the two sets of simulations, in terms of the relations explored in this paper.

Halos in both simulations have been identified using Amiga's Halo Finder (AHF; Knollmann & Knebe 2009), where their masses are defined as the mass inside a sphere containing $\Delta_{\rm vir} \simeq 350$ times the cosmic background matter density at redshift z=0.

The analysis of the simulation data was largely performed using the open source PYNBODY package (Pontzen et al. 2013).

The properties of the simulated galaxies are presented in Table 1. The MaGICC simulations are 12 disk galaxies, separated into two sub-sets labelled as Milky-Way (MW) and irregular (Irr) type galaxies, although they all are disc galaxies with stellar masses ranging from 1×10^{8}-5×10^{10}M$_{\odot}$. From the CLUES simulation we have selected the halos that satisfy the following conditions: (i) Not a sub-halo, (ii) $M_{\rm halo}>4\times10^{10}M_{\odot}$. These integrate a sample of 10 well resolved isolated galaxies. Since this is a Local Group simulation, the three most massive galaxies are loose analogues of the Milky Way, M31 and M33, and the rest are isolated dwarf galaxies.

3 RESULTS

We emphasise the MaGICC set of simulations by showing each individual galaxy in colour in all plots. This is because these galaxies have been thoroughly explored in the literature, as noted in the introduction. The CLUES simulations have not been as extensively analysed in other contexts, and are shown as grey dots. Considering that our results emphasise the ability of the suite of simulations to match various relations, and that one may expect any differences in the two sets of simulations to increase any scatter found around the relations we explore, we feel that it is justified to include all galaxies in the derived results. Thus, our fits include all simulated galaxies. Nothing in our conclusions changes if only MaGICC galaxies are included, although the number and diversity of galaxies would be less.

3.1 Circular velocity curves

Figures 1 and 2 show the gaseous (triangles), stellar (stars), baryonic (squares) and total (circles) circular velocity curves of the MaGICC and CLUES simulated galaxies, respectively. These are measured at radii ranging from 0.7kpc to $10\times h$ where h is the disc scale length (see Table 1). These circular velocities are calculated using the gravitational potential along the midplane of the aligned simulated disc. We checked that our results are not significantly changed by assuming a spherical potential and averaging the mass within spherical shells (i.e., the classical GM/r potential).

The simulated galaxies reach a flat value of circular velocity which persists to large radii, and lack the strong peak at small radii that not so long ago was ubiquitous in simulations due to overcooling. A couple of galaxies, g5664_MW and C1, do have significant bulges, which is reflected in the heightened inner region of their circular velocity curves.

The differences in the physical modelling and initial conditions used in both simulations are not readily visible, with galaxies of similar masses reaching similar maximum, flat velocities (see for example g7124_MW & C3, g15807_Irr & C1 or g5664_Irr & C10). However, there does appear to be a tendency for the MaGICC galaxies to have more slowly rising rotation curves than the

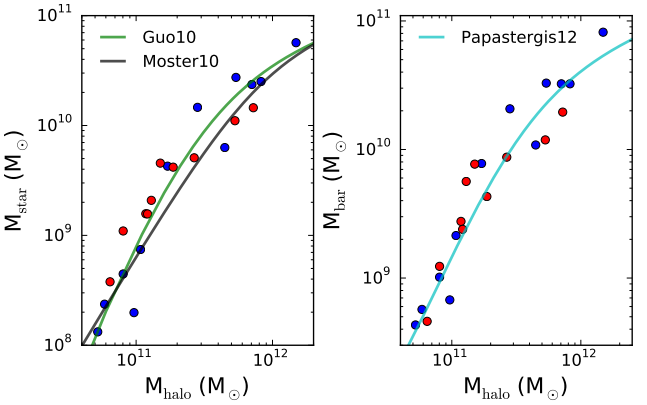

Figure 3. The stellar-to-halo mass (left panel) and baryon-to-halo mass (right panel) relations, with MaGICC galaxies in blue and CLUES galaxies in red. Also shown are the empirical stellar-halo mass relations from Guo et al. 2010 (green line) and Moster et al. 2010 (black line), and the baryon-to-halo mass relation from Papastergis 2012 (cyan line).

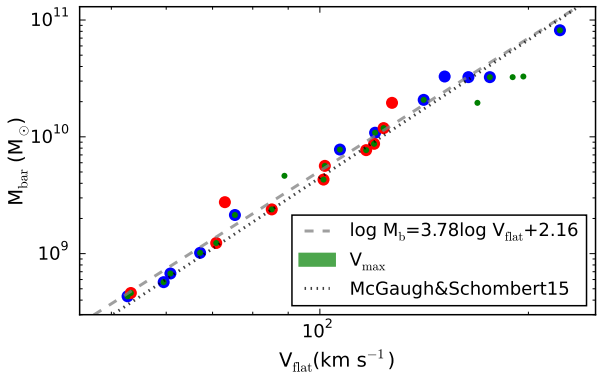

Figure 4. The baryonic Tully-Fisher relation: total baryonic mass M_{bar} (stars + cold gas) plotted against rotation velocity V_{flat}. Blue points are from the MagiCC suite while the red points are the galaxies from the CLUES simulation. The dashed line shows the linear fit to the simulated data, with slope=3.78. The small green points show V_{max} rather than V_{flat}, which results in a slightly flatter relation, with slope=3.49 (see text for details). The dotted line is the observational relation using measurements in the V band given in McGaugh & Schombert 2015 with slope=3.92.

CLUES simulations. The broad range of observed rotation curve shapes has been noted for some time (e.g. Zwaan et al. 1995; Swaters et al. 2009), with recent attempts to quantify this range (Oman et al. 2015; Brook 2015) and compare with cosmological models. The relatively small number of galaxies of each different suite used in this study means it is difficult to compare with observations in a quantitative manner. Whether a larger suite of cosmological simulations can match the range of observed rotation curve shapes will be explored in a later study (Santos-Santos et al. in prep). For this study, we note that there may be slight systematic differences between the MaGICC and CLUES rotation curves shapes, which we will explore in terms of the mass discrepancy relation, and will be seen to be relatively minor.

Visually, one can appreciate that overall, the simulations do produce diversity in rotation curve shapes, and that the baryon contribution increases with increasing mass. One can also see that features from the baryonic components are often reflected in the total-components curves. This is known as "Renzo's Rule" (Sancisi 2004; McGaugh 2014), and has long been observed in real galaxies. In particular, these bumps and features are noticeable in galaxies g15807_Irr, g15784_Irr, g1536_MW, g5664_MW of Figure 1, and C1, C5, C6, C7 & C8 of Figure 2. These results represent evidence that the different mass components affect each other throughout the disc region as they co-evolve within a ΛCDM Universe.

3.2 Baryonic and Halo Masses

In the left panel of Figure 3 the stellar-to-halo mass relation of the simulations is plotted, along with the empirical relation as determined by Guo et al. (2010) and Moster et al. (2010), whilst in the right panel of Figure 3 the baryon-to-halo mass relation is plotted, along with the empirical relation as determined by Papastergis et al. (2012). The baryonic mass is defined as the sum of the mass coming from stars and cold gas particles, where the latter is estimated as a multiple of the atomic HI gas mass $M_g = \eta M_{HI}$, with $\eta = 4/3$ (following e.g. McGaugh 2012). The Saha equation is solved to determine an ionization equilibrium and the HI mass. This remains an approximation since an accurate model of HI mass would require full radiative transfer. In particular self shielding from the UV background is not included in our model and may affect our derived HI masses, while photo-ionization of HI from the galaxy itself is also excluded.

As stated in Section 2, the MaGICC simulations were tuned to match the stellar mass-halo mass relation at one galaxy mass (in particular, to match the stellar to halo mass of galaxy g15784_Irr), and shown to then match the relation over a range of masses (Brook et al. 2012b; Obreja et al. 2014, see also the Nihao simulations, Wang et al. 2015, which use very similar implementation of physics, and note that other models are also able to match the relation, e.g. Munshi et al. 2013; Schaye et al. 2015). The CLUES simulations were also calibrated to match the relation. So, although in some sense it is not surprising that the simulations match the relation to which they were tuned, they actually match the relation over a far wider mass range than the one on which the parameter search was performed.

We show that the simulations also match the empirical M_b-M_{halo} relation, implying that they also have the same total amount of cold gas as observed galaxies at $z = 0$. As far as we know, this is the first time that simulations have been shown to match this important empirical relation, and emphasise that it was not a direct result of a parameter search.

3.3 The Baryonic Tully-Fisher relation

The maximum velocity found in each simulated galaxy, V_{max}, is a good approximation of the flat velocity, V_{flat}, in most cases. For the cases mentioned above in which a couple of MW type galaxies have significant bulges, we show different values of V_{max} and V_{flat} in Table 1.

In Figure 4 we plot the BTFR using V_{flat}, with the MaGICC and CLUES sets of simulations shown as blue and red dots, respectively. In the case of C7, the galaxy is about to undergo a merger, and we use the maximum velocity from the inner 10 kpc as V_{flat} which is the central galaxy, and use the baryonic mass from within this same radius. The fit to the V_{flat} BTFR is

$$\log M_b = 3.78 \log V_{flat} + 2.16$$

The scatter is very small, with the galaxy that is furthest from the

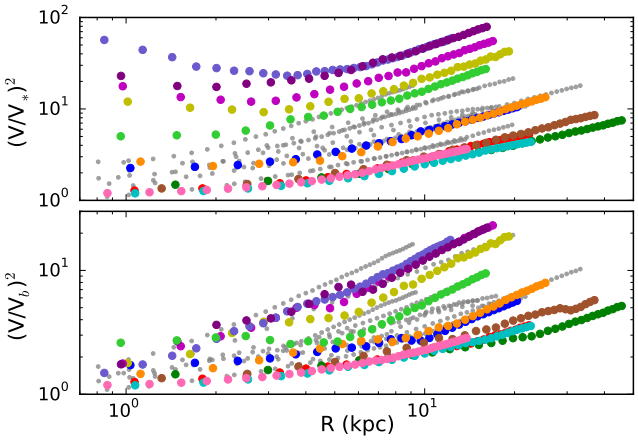

Figure 5. Mass discrepancy versus radius (stars, top panel; all baryons, lower panel). Data points for each MaGICC galaxy are represented in a different color according to figure 1. Data points for all CLUES galaxies are small dots in gray color (as in figure 2). As occurs with observed galaxies, the lower the surface brightness of the galaxy the higher the mass discrepancy encountered: mass discrepancy does not hold a correlation with radius. Smaller values of D are found when all baryons are taken into account as expected.

fit being C7, the one which has a very close companion galaxy with which it is dynamically interacting.

If we simply use V_{max} in each case, the relation is slightly flatter, and can be seen as small green dots in Figure 4, with fit

$$\log M_b = 3.49 \log V_{max} + 2.67$$

and similar scatter.

These fits are consistent with the observational fits found in the literature (see McGaugh 2012, for a summary), as is the trend for a flatter relation when using V_{max} rather than V_{flat}.

3.4 Mass discrepancy

"Mass discrepancy" refers to the difference between the total mass and the baryonic mass enclosed at a certain radius, which can be inferred from the rotation curve of a galaxy. The value of the mass discrepancy D is calculated as the squared ratio of the observed velocity to that due to the observed baryons $D=(V_r/V_b)^2$.

Figure 5 shows mass discrepancy plotted against radius, each point representing a point along the rotation curves (MaGICC galaxies are colored points, CLUES are small gray dots). In the upper panel mass discrepancy is computed as the squared ratio of the observed velocity to that predicted by the stars, and in the lower panel all baryons (stars plus cold gas) are taken into account.

At the radii where D=1, the rotation of the galaxy can be explained by the contribution of baryons (stars in the upper panel) alone, while the mass discrepancy (need for dark matter) appears when D>1. As with observed galaxies, the mass discrepancy does not appear at the same radius for all galaxies, and increases with radius but not at a constant rate for every system (McGaugh 2014). Furthermore, galaxies separate readily when mass discrepancy is plotted against radius, with low mass galaxies having a larger dark matter contribution to the mass at any given radius, compared to higher mass galaxies.

We note the most prominent difference between simulations and observations for the relations shown in Figure 5 is that $(V/V_b)^2$ is higher at low radii for the lowest mass observations, than for the

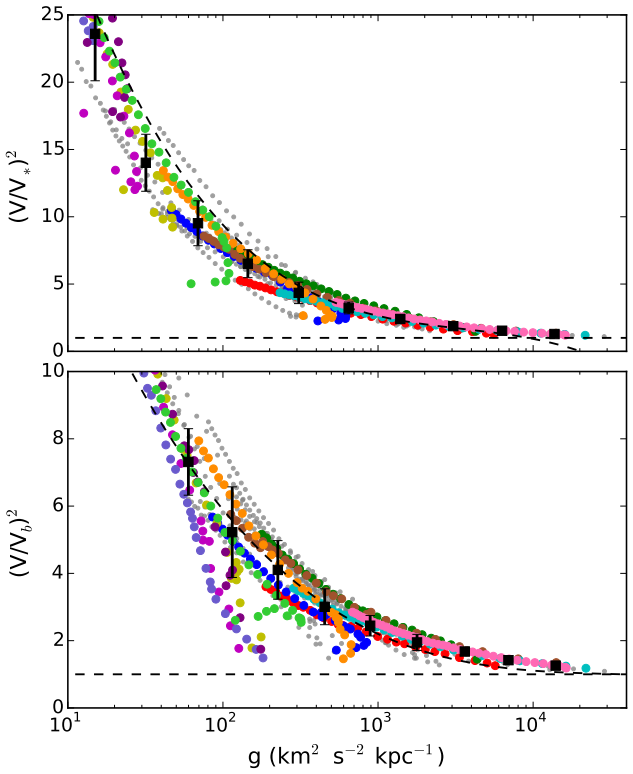

Figure 6. Mass discrepancy versus acceleration produced by stars (top panel), and by all baryons–stars + cold gas–(lower panel). The 22 galaxies are shown with colors as in Figures 1 and 2. The dashed lines are the observational D-g relations (equations 8 & 9 of McGaugh 2014). An horizontal dashed line is also shown in both panels to emphasize the asymptotic behaviour of the relation to D=1. Binned data is shown as black squares. The errors are the *rms* deviations from the best 3 degree polynomial fit found for the data in each bin.

corresponding data from the simulations. As this difference does not appear in the $(V/V_*)^2$ case, one may infer that the simulations have an excess of cold gas in the inner regions of low mass galaxies.

Figure 6 shows the mass discrepancy-acceleration relation for all the simulated galaxies, where the acceleration is derived from the gravitational potential of the stars (top panel) and baryons (lower panel), $g \equiv V^2/r$. In this plot, since radius is inversely proportional to the gravitational acceleration, an increase in radius along a rotation curve is read from right to left. One can observe that more massive galaxies reach higher values of g. Note that although individual galaxies inhabit different regions of the plot, as can be readily seen for the MaGICC set which are plotted as different colors, they all follow a single relation.

We divide the data in 10 bins and show in Figure 6 the fit to the data in each bin as black squares. Error bars show the standard deviation within each bin. Dashed lines represent the fits found for observational data, using equations 8 & 9 of McGaugh (2014).

A slight deviation from the general trend can be seen at $g \sim 10^2$ and $D \sim 2$, with some points of the simulated galaxies falling below the D-g relation. This feature is also seen in the observed mass discrepancy–acceleration relations. In the simulations, it is specially evident for MaGICC galaxies g21647_Irr, g7124_Irr, g5664_Irr and g1536_Irr in the "all baryons" relation. These are the galaxies that have the most slowly rising rotation curves, as mentioned in section 3.1. As discussed above, the stronger feedback scheme present in these simulations removes more baryonic mass

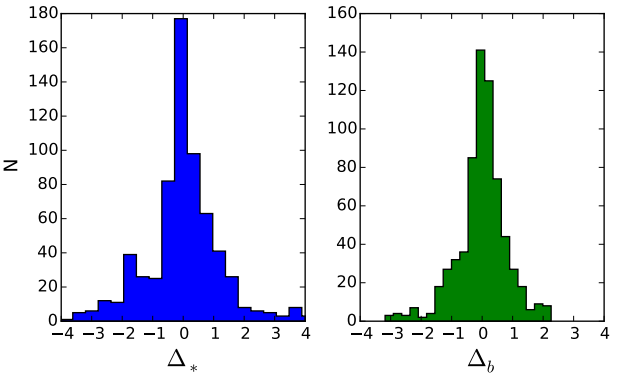

Figure 7. Histograms of the residuals around the fits. Left: only stellar contribution; Right: all baryons.

from the centre of some of the simulated galaxies, causing the velocity in this inner region to be lower than expected by the one-to-one D-g relation. Better statistics are required to determine whether the deviations from the relation seen in the simulations are more or less prominent than seen in the observations, and may relate to the observed diversity of rotation curve shapes.

Another possible difference between the observations and simulations is found in the baryonic D-g relation, where the observed galaxies extend down to D=1, while the simulated galaxies do not quite reach this asymptotic value. Comparing such fine details of the relations would likely require better matched observational and simulated data, in terms of the distributions of stellar masses and scale-lengths. In particular, the observed sample appears to have more massive disc galaxies, which may be dominated by baryons in the inner region and hence extend down to lower values of D than the simulated sample, which has only 1 galaxy with $M_* > 3\times10^{10} M_\odot$.

The intrinsic scatter we find with respect to the fit in each bin, as well as the deviation from the observed relations, is small and decreases as D tends to 1. In Figure 7 the histograms of the residuals found around the fits are shown to be narrow, with a very similar spread to that of observed galaxies.

4 CONCLUSIONS

In this paper we have moved beyond using the Tully-Fisher relation as a test of the angular momentum content of galaxies simulated in a ΛCDM cosmological context, to include the wealth of information contained within extended rotation curve data. We do this by exploring the mass discrepancy-acceleration relation through the full radial range of the disc in each of 22 simulated galaxies, a suite that spans more than two orders of magnitude in stellar mass, with rotation velocities ranging from 52 to 222 km s^{-1}.

The simulated suite of late type galaxies is shown to match the empirical relation between baryonic mass, which includes their stars and cold gas, and halo mass, as well as the baryonic Tully-Fisher relation.

Despite showing significant diversity in the shapes of their rotation curves, and in the contribution of dark matter to the total mass budget, the simulated galaxies follow a single relation in both the D-g_* and D-g_b plots, with small scatter. The implication is that not only the total amount of angular momentum attained by the simulated galaxies is correct, as shown by the BTFR, but also that their final internal distribution of gas, stars and dark matter at all radii through their discs is similar to that observed in real galaxies.

The acquisition of the angular momentum within the simulations is complicated, as compared to the simple models of angular momentum acquisition within a CDM universe that assume collapsing spheres of gas, torqued by large scale structure (Fall & Efstathiou 1980). The baryon cycle within the simulated discs studied here (see Brook et al. 2014, for details) involve a complex web structure, large scale outflows of low angular momentum gas (Brook et al. 2011), and redistribution of low angular momentum gas through large scale galactic fountains (Brook et al. 2012a). Further, the dark matter distributions respond to the gas flows in a manner that is dependent on the simulated galaxy mass (Di Cintio et al. 2014b,a).

Yet in many ways, our model remains straight forward once the ΛCDM initial conditions are set, with much of the physics involved in driving the complicated galactic scale baryon cycle occurring on "sub-grid" scales, and accounted for by using relatively simple prescriptions. These prescriptions have improved markedly over the past decade, such that we are able to simulate populations of galaxies that have global properties similar to observed galaxy populations. Our study shows that the distribution of mass within disc galaxies with a wide range of masses and rotational velocities can now also be well reproduced within a ΛCDM universe.

ACKNOWLEDGEMENTS

We thank Yehuda Hoffman for making the CLUES initial conditions available. ISS, CB & GY thank the MINECO (Spain) for the financial support through the AYA2012-31101 grant. CB is funded through the Ramon y Cajal program of the MINECO. The CLUES simulations were performed and analyzed at the High Performance Computing Center Stuttgart (HLRS). We thank DEISA for access to computing resources through DECI projects SIMU-LU and SIMUGAL-LU and the generous allocation of resources from STFCs DiRAC Facility (COSMOS: Galactic Archaeology), the DEISA consortium, co-funded through EU FP6 project RI-031513 and the FP7 project RI-222919 (through the DEISA Extreme Computing Initiative), the PRACE-2IP Project (FP7 RI-283493).

REFERENCES

Aumer M., White S. D. M., Naab T., Scannapieco C., 2013, MNRAS, 434, 3142
Barnes J., Efstathiou G., 1987, ApJ, 319, 575
Begeman K. G., Broeils A. H., Sanders R. H., 1991, MNRAS, 249, 523
Brook C., 2015, arXiv.1506.00214
Brook C. B. et al., 2011, MNRAS, 595
Brook C. B., Stinson G., Gibson B. K., Roškar R., Wadsley J., Quinn T., 2012a, MNRAS, 419, 771
Brook C. B., Stinson G., Gibson B. K., Shen S., Macciò A. V., Obreja A., Wadsley J., Quinn T., 2014, MNRAS, 443, 3809
Brook C. B., Stinson G., Gibson B. K., Wadsley J., Quinn T., 2012b, MNRAS, 424, 1275
Cantalupo S., 2010, MNRAS, 403, L16
de Blok W. J. G., McGaugh S. S., Bosma A., Rubin V. C., 2001, ApJ, 552, L23
Di Cintio A., Brook C. B., Dutton A. A., Macciò A. V., Stinson G. S., Knebe A., 2014a, MNRAS, 441, 2986

Di Cintio A., Brook C. B., Macciò A. V., Stinson G. S., Knebe A., Dutton A. A., Wadsley J., 2014b, MNRAS, 437, 415
Doménech-Moral M., Martínez-Serrano F. J., Domínguez-Tenreiro R., Serna A., 2012, MNRAS, 421, 2510
Domínguez-Tenreiro R., Obreja A., Brook C. B., Martínez-Serrano F. J., Stinson G., Serna A., 2015, ApJ, 800, L30
Fall S. M., Efstathiou G., 1980, MNRAS, 193, 189
Feldmann R., Mayer L., 2015, MNRAS, 446, 1939
Gentile G., Salucci P., Klein U., Vergani D., Kalberla P., 2004, MNRAS, 351, 903
Gottloeber S., Hoffman Y., Yepes G., 2010, arXiv.1005.2687
Governato F. et al., 2010, Nature, 463, 203
Governato F. et al., 2004, ApJ, 607, 688
Guedes J., Callegari S., Madau P., Mayer L., 2011, ApJ, 742, 76
Guo Q., White S., Li C., Boylan-Kolchin M., 2010, MNRAS, 404, 1111
Hopkins P. F., Kereš D., Oñorbe J., Faucher-Giguère C.-A., Quataert E., Murray N., Bullock J. S., 2014, MNRAS, 445, 581
Kannan R., Stinson G. S., Macciò A. V., Brook C., Weinmann S. M., Wadsley J., Couchman H. M. P., 2013, arXiv.1302.2618
Kannan R. et al., 2014, MNRAS, 437, 2882
Knollmann S. R., Knebe A., 2009, ApJS, 182, 608
Kuzio de Naray R., McGaugh S. S., de Blok W. J. G., Bosma A., 2006, ApJS, 165, 461
Maller A. H., Dekel A., 2002, MNRAS, 335, 487
McGaugh S., 2014, Galaxies, 2, 601
McGaugh S. S., 2004, ApJ, 609, 652
McGaugh S. S., 2005, ApJ, 632, 859
McGaugh S. S., 2012, AJ, 143, 40
McGaugh S. S., Schombert J. M., 2015, ApJ, 802, 18
Milgrom M., 1983, ApJ, 270, 365
Moster B. P., Naab T., White S. D. M., 2013, MNRAS, 428, 3121
Moster B. P., Somerville R. S., Maulbetsch C., van den Bosch F. C., Macciò A. V., Naab T., Oser L., 2010, ApJ, 710, 903
Munshi F. et al., 2013, ApJ, 766, 56
Navarro J. F., Steinmetz M., 2000, ApJ, 538, 477
Obreja A., Brook C. B., Stinson G., Domínguez-Tenreiro R., Gibson B. K., Silva L., Granato G. L., 2014, MNRAS, 442, 1794
Oh S.-H. et al., 2015, arXiv.1502.01281
Oman K. A. et al., 2015, arXiv.1504.01437
Papastergis E., Cattaneo A., Huang S., Giovanelli R., Haynes M. P., 2012, ApJ, 759, 138
Peebles P. J. E., 1969, ApJ, 155, 393
Pichon C., Pogosyan D., Kimm T., Slyz A., Devriendt J., Dubois Y., 2011, MNRAS, 418, 2493
Piontek F., Steinmetz M., 2011, MNRAS, 410, 2625
Pontzen A., Roškar R., Stinson G. S., Woods R., Reed D. M., Coles J., Quinn T. R., 2013, pynbody: Astrophysics Simulation Analysis for Python. Astrophysics Source Code Library, ascl:1305.002
Prochaska J. X., Weiner B., Chen H.-W., Mulchaey J., Cooksey K., 2011, ApJ, 740, 91
Rubin V. C., Ford, Jr. W. K., 1970, ApJ, 159, 379
Sancisi R., 2004, in IAU Symposium, Vol. 220, Dark Matter in Galaxies, Ryder S., Pisano D., Walker M., Freeman K., eds., p. 233
Sanders R. H., McGaugh S. S., 2002, ARA&A, 40, 263
Sanders R. H., Verheijen M. A. W., 1998, ApJ, 503, 97
Schaye J. et al., 2015, MNRAS, 446, 521
Shen S., Wadsley J., Stinson G., 2010, MNRAS, 407, 1581
Stinson G., Seth A., Katz N., Wadsley J., Governato F., Quinn T., 2006, MNRAS, 373, 1074
Stinson G. S., Bailin J., Couchman H., Wadsley J., Shen S., Nickerson S., Brook C., Quinn T., 2010, MNRAS, 408, 812
Stinson G. S., Brook C., Macciò A. V., Wadsley J., Quinn T. R., Couchman H. M. P., 2013, MNRAS, 428, 129
Stinson G. S. et al., 2012, MNRAS, 425, 1270
Swaters R. A., Sancisi R., van Albada T. S., van der Hulst J. M., 2009, A&A, 493, 871
Thacker R. J., Couchman H. M. P., 2001, ApJL, 555, L17
Tully R. B., Verheijen M. A. W., 1997, ApJ, 484, 145
Tumlinson J. et al., 2011, Science, 334, 948
van den Bosch F. C., Dalcanton J. J., 2000, ApJ, 534, 146
Wadsley J. W., Stadel J., Quinn T., 2004, NewA, 9, 137
Wang L., Dutton A. A., Stinson G. S., Macciò A. V., Penzo C., Kang X., Keller B. W., Wadsley J., 2015, arXiv.1503.04818
Yepes G., Gottlöber S., Hoffman Y., 2014, New Astron. Rev., 58, 1
Zwaan M. A., van der Hulst J. M., de Blok W. J. G., McGaugh S. S., 1995, MNRAS, 273, L35